AN ABSTRACT OF THE THESIS OF

<u>Kenneth J. Squire</u> for the degree of <u>Master of Science</u> in <u>Electrical and Computer Engineering</u> presented on <u>September 13, 2017.</u>

Title: <u>Multi-Modal Biosensing with Diatom Photonic Crystal Biosilica</u>

Abstract approved: _____

Alan X. Wang

The need to detect trace amounts of target molecules is great, particularly when it comes to biosensing. With the early detection of a disease, the odds of the successful treatment of an individual increases significantly. To enhance the capability of biomolecular detection, we have created an optical biosensor capable of the enhancement of multi-modal optical signals. Our substrate employs diatoms, a type of algae, with unique optical properties to achieve multi-modal enhancement. Diatom shells, called frustules, are made of biosilica with quasi-periodic pores. These frustules exhibit a very large surface area which allows for a large area of interaction for analytes. Additionally, the porous structure of the frustule acts as a photonic crystal capable of enhancing optical signals. Here we demonstrate the multi-modal enhancement capabilities of our biosensor through the detection of biological analytes using colorimetric shifts, surface enhanced Raman scattering and fluorescence biosensing.

Multi-Modal Biosensing with Diatom Photonic Crystal Biosilica

by
Kenneth J. Squire

A THESIS

submitted to

Oregon State University

in partial fulfillment of
the requirements for the
degree of

Master of Science

Presented September 13, 2017
Commencement June 2018

Master of Science thesis of Kenneth J. Squire presented on September 13, 2017

APPROVED:

_____

Major Professor, representing Electrical and Computer Engineering

_____

Director of the School of Electrical Engineering and Computer Science

_____

Dean of the Graduate School

I understand that my thesis will become part of the permanent collection of Oregon State University libraries. My signature below authorizes release of my thesis to any reader upon request.

_____

Kenneth J. Squire, Author

ACKNOWLEDGEMENTS

I would like to thank my advisor Dr. Alan Wang for his support for the past couple years. His guidance and teaching were instrumental in the fulfillment of this work. His encouragement helped me to reach new heights in my professional development and taught me how to perform research. I would also like to thank Dr. Larry Cheng, Dr. Matthew Johnston, Dr. Gregory Rorrer and Dr. Karl Schilke for serving on my committee. Thank you for your time and support.

My labmates have helped me immensely throughout this process and have become my close friends. Thank you for your help with experiments, measurements, writing, and everything else. I would especially like to thank Dr. Xianming Kong who mentored me as I began studying biosensors in everything from wet chemistry to best practices for research. I hope you continue to have success.

Thank you to my parents and family for their continued support and interest in my research. Lastly, I would like to thank my wife, Stephanie, for her support and encouragement. She has weathered many lonely nights and weekends while I was pursuing this degree and when I would hit a wall, her support helped me to persevere and accomplish my goals. Thank you, I love you.

TABLE OF CONTENTS

TABLE OF CONTENTS (Continued)

LIST OF FIGURES

LIST OF FIGURES (Continued)

1. Introduction

1.1 Optical Biosensor Technology

The use of biosensors to ensure early detection of harmful agents and diseases can greatly increase the chances of successful containment and treatment. The mechanisms employed by biosensors range from sensing a change in electrical current to a chemical change inducing a change in voltage. However, one type of biosensor that has grown in prevalence and variety of application is optical biosensors. Optical biosensors have found application in a variety of fields including detection of pesticides and chemical warfare agents[1], cancer[2], and water contamination[3] to name a few. Optical biosensors operate by sensing a change in intensity, spectrum, or color of measured light transmitting through or reflected from a sample. In each of these methods the sensor is characterized by its sensitivity and selectivity.
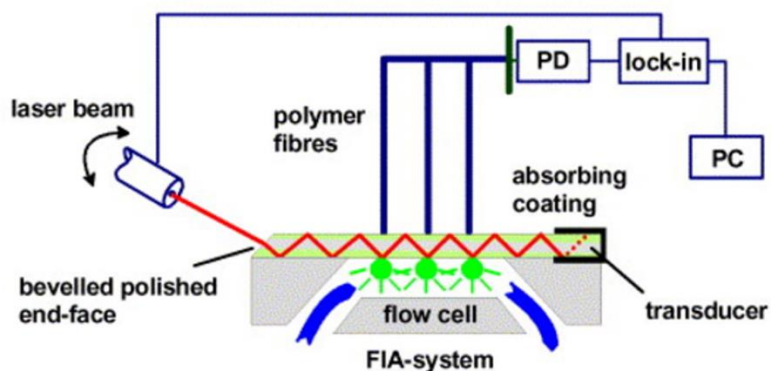
Figure 1: Optical biosensor where a flow cell is used to deliver the sample near the sensing surface where the analyte induces a decrease in laser intensity. The laser light is extracted through fiber optics and measured using a photodiode[3].

The sensitivity of a sensor is a measure of the output signal in relation to the input. A sensor with higher sensitivity will produce a greater change in output signal than a less sensitive sensor when both have the same input. Highly sensitive sensors allow the detection of low amounts of their target which allows for earlier detection. A sensor's selectivity denotes the ability to detect a target signal when in the presence of competing signals. Greater selectivity allows a sensor to be used in harsher environments where the signal may be otherwise obscured by noise. Different optical mechanisms of detection have advantages and disadvantages but the goal is to maximize the sensitivity and selectivity for a given application. Some common methods of optical biosensing are colorimetric sensing, surface-enhanced Raman spectroscopy, and fluorescent biosensing.

1.2 Colorimetric Biosensing

Colorimetric biosensing operates on the principle that the sensor will change colors when the target is present. This color shift is generally accomplished using metal nanoparticles (NPs). When NPs are excited with a light source, the NPs absorb some of the light and standing waves are generated on the surface of the particle. These standing waves are called surface plasmons. A change in the refractive index of the environment immediately around the NPs causes a change in the absorption spectrum of the NP thereby generating a change in perceived color. By measuring the absorption spectrum before and after the sensing event, one can detect the analyte. The sensor's change in color can be analyzed by a variety of methods. The sensor can

implement one, or a combination of these methods. One method is to visually compare the color of the sensor to a reference chart to achieve semi-quantitative results. This method is convenient for point-of-care detection and can be used without the need of expensive sensing instrumentation or trained technicians. This technique has been used to detect DNA-binding protein[4], pesticides on vegetables[5], small amounts of mercury ions[6], and glucose in urine[7].
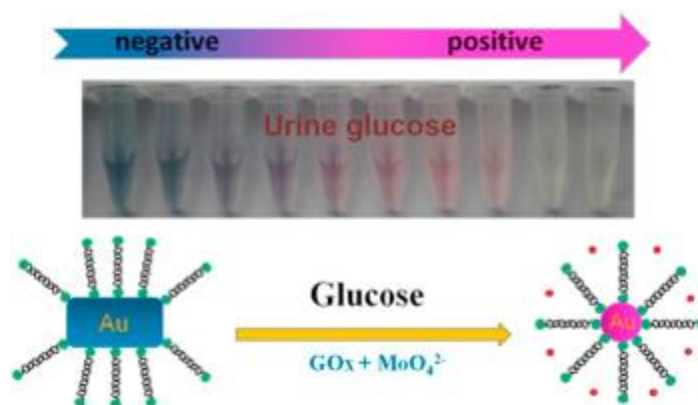
Figure 2: Colorimetric biosensor detecting various concentrations of glucose in a sample experiences a color change ranging from blue to clear based on the concentration of glucose in the sample[7].

A second method of analysis implements a spectrometer to measure the absorption peak before and after a detection event. The binding event induces a shift in the absorption peak which can be quantitatively determined using a spectrometer. The amount of shift correlates to the amount of analyte present in a sample. This method is often used with known quantities of analyte to create the reference charts used for the visual detection method described above.

Another colorimetric detection method is similar to that just described but rather than using a spectrometer, a camera is used. Instead of measuring the absorption spectrum, a picture is taken

before and after the binding event. By analyzing the picture, a quantifiable change in color can be calculated. This color change is due to a change in the peak absorption and can be used to determine the concentration of analytes in a sample. This approach has gained increased interest with the technological advancement of smartphone cameras. Using smartphone paired colorimetric sensors glucose[8], e. coli[9], and explosives[10] have successfully been detected.

The sensitivity for colorimetric sensing comes from the change of refractive index that can be induced in the environment immediately around the NP as well as the NPs sensitivity to that change. The selectivity comes from the chemical surface functionalization of the NPs. By engineering these parameters, the selectivity and sensitivity of a colorimetric biosensor can be optimized.

1.3 Surface-Enhance Raman Spectroscopy

Surface-enhanced Raman spectroscopy relies on Raman scattering to detect and identify a target. When a sample is excited by a laser light source, some of the scattered light is shifted from the original wavelength. This shifted scattering, called Raman scattering, arises from the inelastic scattering of light off molecules. The different chemical bonds in a sample have different Raman peaks with different intensities. Thus, the Raman signal measured is a unique fingerprint of a material and allows for highly specific sensing. However, the amount of Raman scattering compared to elastic scattering is extremely low. To utilize the highly specific nature of Raman scattering, the Raman signal must be greatly enhanced. Surface-enhanced Raman scattering

(SERS) is a field of study that has quickly grown to take advantage of the specificity of Raman. Using SERS, enhancement factors of the Raman signal of up to 10^{14} or 10^{15} have been achieved[11] as well as single molecule detection[12].
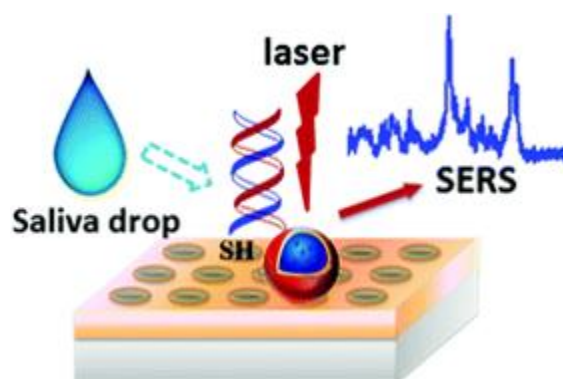
Figure 3: SERS biosensor where the sample is administered and a SERS signal is achieved by laser light excitation[13].

SERS is achieved by enhancing the localized electromagnetic field. This is done by creating localized surface plasmon resonance (like the plasmons discussed in the colorimetric section) on a metal surface with nanoscale features[14]. Many different SERS substrates have been investigated to achieve this plasmon resonance. Common SERS substrates include utilization of gold, silver or copper to fabricate NPs[15,16], thin films[17,18], and other nanostructures[19,20].

SERS sensitivity is dependent on the Raman signal of the target molecule, the Raman microscope used, and the metal nanostructure used to enhance the Raman signal. The selectivity comes from the functionalization of the SERS substrate and the matrix of your sample. Where many other biosensors excel in detecting the presence of a molecule, SERS is not only able to detect, but also able to identify a molecule attached to the substrate due to the unique SERS spectrum.

1.4 Fluorescent Biosensing

The basic mechanism of fluorescent biosensing is that a fluorescent molecule, called a fluorophore, absorbs light at one spectrum of wavelengths and reemits the light at a different spectrum. This mechanism can be employed in a variety of ways. One method of fluorescent biosensing is to have fluorophores on a substrate and then functionalize the substrate in such a way that the target molecule binds near the fluorophore. The analyte then either quenches the fluorescent signal or replaces the fluorophore. By comparing the fluorescent signal with and without the target present, quantitative results can be obtained. This "turn-off" method has been applied to a variety of fields including the detection of mercury[21,22] and glucose[23].
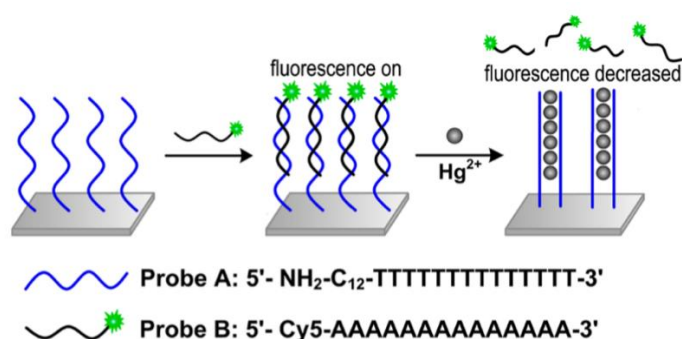
Figure 4: Fluorescent turn-off sensor to detect mercury. The fluorescent signal is "on" until mercury is introduced. When the mercury releases the bond between probe A and probe B, the fluorescence decreases[22].

Another fluorescent biosensing method is the creation of an immunoassay sandwich. In this approach, a substrate is prepared with a primary antibody attached to the surface. The sensing sample is then placed on the substrate and the target molecule binds to the primary antibody

and remains on the substrate as the rest of the sample is washed off. The same primary antibody, tagged with a fluorophore, is introduced to the substrate. The fluorophore-tagged antibody binds to the target molecule thus creating a sandwich. Once the immunoassay procedure has occurred, the sample is illuminated by a light source to excite the fluorophore. Quantitative results can be obtained by measuring the intensity of the fluorophore emission. Using this sandwich approach researchers have achieved detection of Salmonella in nutrient broth[24], Escherichia coli in ground beef[25], and cancer biomarkers[26].
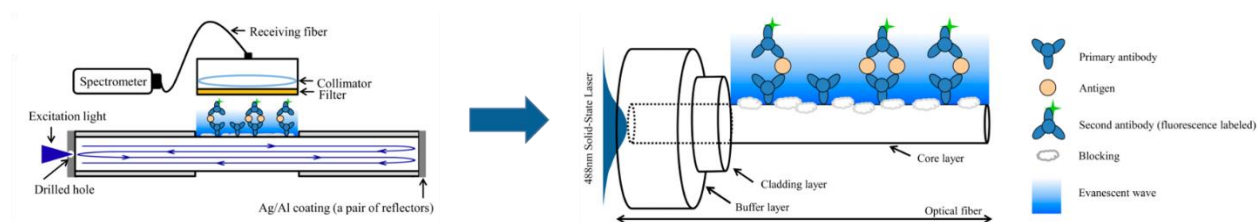
Figure 5: Example of fluorescent biosensing based on the sandwich immunoassay. On the left, the biosensing system is shown where a section of fiber is stripped of the cladding, functionalized with antibodies and then illuminated using a laser. The light interacts with the sample through the exposed area, goes through a filter and into a spectrometer. On the right, the exposed region is shown with the sandwich immunoassay[27].

The selectivity of fluorescent biosensing is dictated by the chemical functionalization that allows the binding of the target to the sensor. The characteristics of the fluorophores such as their ability to bind to the substrate and target, the sensitivity to their environment and ability to be quenched, and the quality of the instrumentation all determine the sensitivity of the fluorescent biosensor.

1.5 Photonic Crystals

Photonic crystals (PCs) are periodic dielectric structures with nanoscale features that can be single or multi-dimensional. One dimensional PCs can be stacked layers of dielectric media with different indices of refraction. Two dimensional PCs can be gratings or structures with a checkerboard structure where the different materials are periodic in two directions. A three-dimensional PC is similar to a three-dimensional checkerboard. These can be fabricated using reactive ion etching[28], lithography[29-31], or direct laser writing[32,33]. Photonic crystals are significant because the periodic refractive index interacts with incident light and can cause resonance that will enhance the electromagnetic field in the PC. Two methods of enhancement are the Purcell effect and guided mode resonance.
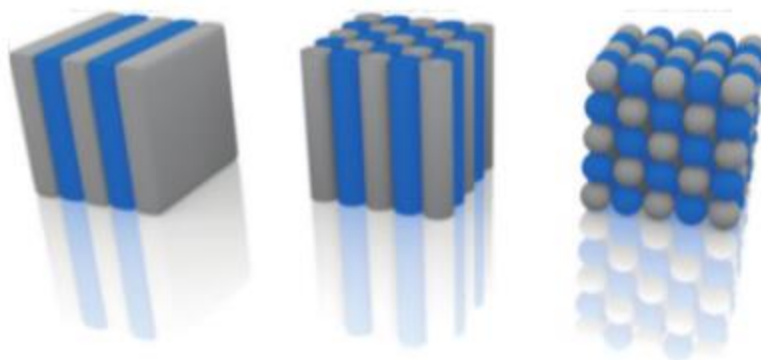
Figure 6: Representation of 1, 2 and 3-D photonic crystals[34].

The Purcell effect causes enhanced fluorescence of fluorophores in a cavity at resonance. This results from an increased optical density of states which in turn speeds up the transition rate[35, 36]. As the transition rate increases, the fluorescent emission increases. The Purcell effect has

been investigated and employed to enhance quantum dot fluorescent emission by as much as 108×[37]. Utilization of the Purcell effect given by photonic crystals in biosensors helps to increase the sensitivity of a biosensor.

Guided mode resonance (GMR) occurs when incident light resonates with the PC. The incident light is coupled into guided modes in the PC that constructively interfere to enhance the electric field compared to the incident light. With an enhanced electric field on the PC, the target molecules will have an enhanced interaction with the light and the signal will be enhanced, and thus improve the sensor's sensitivity.

1.6 Recent Innovations of Photonic Crystal based Biosensors

The applications of PCs to biosensors are varied as are the methodologies employed. One research group has measured HIV in serum and buffer solution. This was achieved by observing the narrowband reflection spectrum from the PC and detecting a shift in the peak reflection[38]. The same group fabricated another sensor that enhances the fluorescent signal to detect cancer biomarkers. By tuning the PC to the excitation wavelength of their fluorophore, the fluorescence was enhanced and thus lower detection limits were achieved[26]. Another group used photonic crystal beads with a gel to create a photonic crystal thin film for colorimetric sensing to detect Hg^{2+}. The colorimetric shift was visually observable but measurements were acquired by measuring the shift in reflected wavelength[39]. The value of PCs in optical biosensors is obvious

but PCs often require expensive instruments for fabrication. An inexpensive solution is needed to make PC biosensors more practical for widespread biosensors.

1.7 Introduction to Diatoms

Diatoms are a type of algae that have biosilica cell walls. These biosilica shells, called frustules, have quasi-periodic pores that form a natural photonic crystal. Diatoms are abundant in the oceans and their frustules represent a natural, inexpensive, biosilica PC. Diatoms have gained a lot of attention in recent years for applications in biosensors[40-42], drug delivery[43-45], and nanotechnology fabrication[46, 47]. Diatoms have received this attention due to a number of major advantages. Firstly, due to their highly porous nature, diatoms have a very large surface area that allow high density binding and concentration of analytes[42]. Second, diatoms are naturally forming photonic crystals affording all the benefits of photonic crystals without the required time consuming fabrication[48]. Lastly, diatoms are naturally occurring and abundant in nature making them inexpensive and easy to acquire. Additionally, it has been shown that diatoms are capable of significantly enhancing optical signals. Some examples of optical enhancement are 4x enhancement of R6G SERS signal[49] and 6× higher sensitivity to immunoassay binding using SERS[50]. The availability, lack of difficult fabrication, and large enhancement from diatoms make them ideal for use in biosensors.
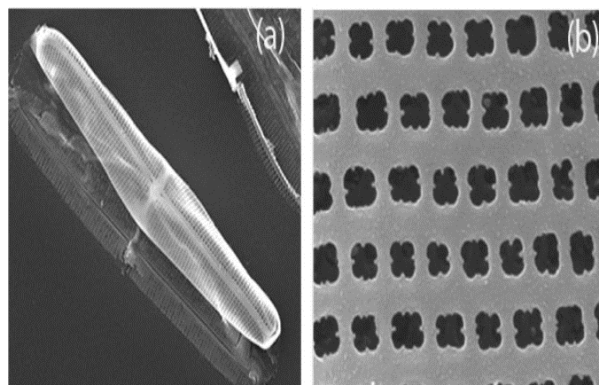
Figure 7: SEM image of (a) total diatom frustule and (b) enlarged image showing the nanoporous structure[16].

2. Diatom Based Colorimetric Biosensor

2.1 Fabrication of Diatom Based Colorimetric Sensor

To prepare the diatom based colorimetric sensor, diatoms were prepared according to the process described in the literature[16]. Briefly, diatoms were cultured for a week after which 400 mL of suspended diatoms were centrifuged and redispersed in 40 mL of artificial seawater. The solution was filtered using a 20 µm mesh to isolate the cells which were then diluted to a density of $2.5 * 10^5$ cells/mL. The cells were pipetted onto glass slides and left to incubate in a humidifier to allow the cells to settle onto the surface. After an hour, the glass substrates were placed in a fresh petri dish and left in the humidifier for another 24 hours. Following incubation in the humidifier, the substrates were placed in 70% ethanol (EtOH) for 4 hours, then placed in 100% EtOH for another 4 hours. The samples were dried and placed in a UV Ozone cleaner at 90˚ C for 24 hours. The substrates were then ready for future use.

After preparing the diatom substrates, gold nanoparticles (Au NPs) with 60 nm diameter were self-assembled onto the substrates. First, the Au NPs were prepared following the procedure described in the literature[51]. As a short explanation, 100 mL of aqueous 1 mM chloroauric acid was first boiled under constant stirring. Next, 4.2 mL of 1% trisodium citrate, a reducing agent, was added to the boiling acid. After several minutes, the yellow solution turned deep purple as the Au began to aggregate. The solution was boiled while refluxing for 20 minutes to allow complete reduction. The solution was cooled to room temperature and was then ready to use.

The colorimetric sensor was prepared by populating a glass slide with diatoms as described followed by annealing at 450° C for 1 hour. The fabrication process includes several chemical processes and is illustrated in figure 8. After each step, the substrate was rinsed thoroughly with Milli-Q deionized water. To briefly describe the process, the slide with diatoms was first immersed in a 1.5% mixture (v/v) of (3-Aminopropyl) triethoxysilane (APTES) and EtOH for 3 hours to achieve silanization. The substrate was then placed in the Au NP solution overnight. The substrate was submerged in 5 mM 3-mercaptopropionic acid (MPA) in water for 4 hours to attach a carboxyl group to the NPs. The carboxyl group was then activated with an amine group with a mixture of equal parts morpholine ethanesulfonic acid (MES) (100mM), 1-Ethyl-3-[3-dimethylaminopropyl] carbodiimide (EDC) (50mM) and N-hydroxysuccinimide (NHS) (50mM) drop cast onto the sample and stored at 4° C overnight. Following the amine group, goat anti-mouse immunoglobulin (IgG) (2 mg/mL) was pipetted onto the substrate and again left at 4° C overnight. 3% bovine serum albumin (BSA) in phosphate-buffered saline (PBS) was then drop cast onto the substrate and left for 4 hours to block the remaining amine groups to prevent non-specific binding. Mouse IgG was then pipetted onto the sensor and allowed to bind overnight at 4° C.
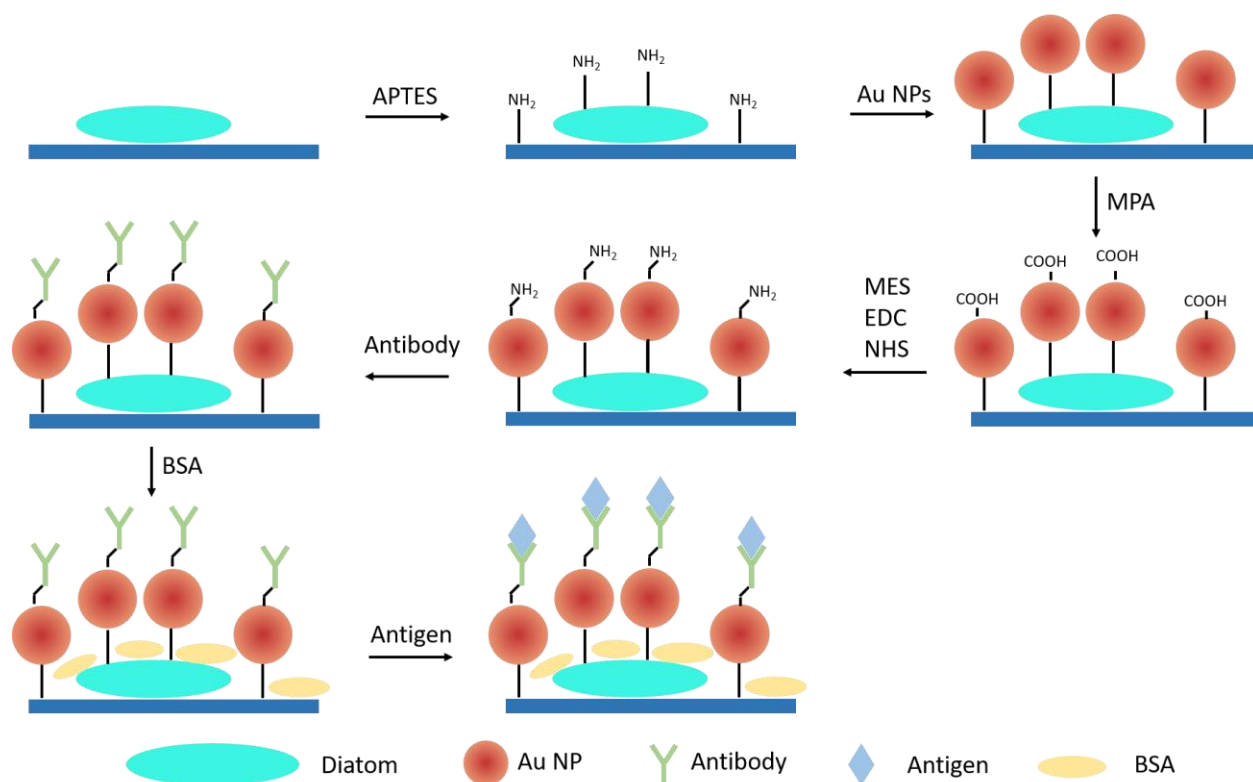
Figure 8: Schematic showing chemical process to create diatom based colorimetric sensor.

2.2 Colorimetric Data Acquisition

The sensor was prepared as described up until the BSA blocking. After the BSA was rinsed off and the sample was dried, a picture was taken of the sample using a microscope with 100× objective lens and a CCD camera. The antigen was then left to bind to the sample and after being rinsed and dried again, a picture was taken of the same diatom. Care was taken to align the sample so it was in the same orientation, focus, and position as the initial image.

2.3 Colorimetric Data Analysis and Results

Matlab was used to analyze each picture pair by first identifying features in each of the images. The post-assay image was then rotated and shifted so that it aligned with the pre-assay image. The pictures taken by the CCD were RGB images and the blue-green ratio (B/G) was used as our metric. The gold nanoparticles used have a peak absorption of 520 nm. The immunoassay binding event of the antibody and antigen shifts that peak to longer wavelengths. As the absorption peak red shifts, we expect the blue value to increase while the green value decreases. This leads to the B/G ratio increasing overall. After the images were aligned, an area on diatom and an equal area on glass were cropped from the images. The images were then placed on a red background which is easily ignored during analysis. The pre-assay diatom section was subtracted from the post-assay diatom section and the same was done for the glass sections. Doing this, we were able to create a shift map that allowed us to visualize the amount of spectral shift between the two images. We performed a hotspot analysis by defining a hotspot as a pixel whose ratio shift was greater than 0.1, and calculating the hotspot density on diatom and glass. This process is shown in figure 9. Using this process, detection of 100 µg/mL of antigen in PBS was achieved and an enhancement factor of 5× due to diatom compared to glass.
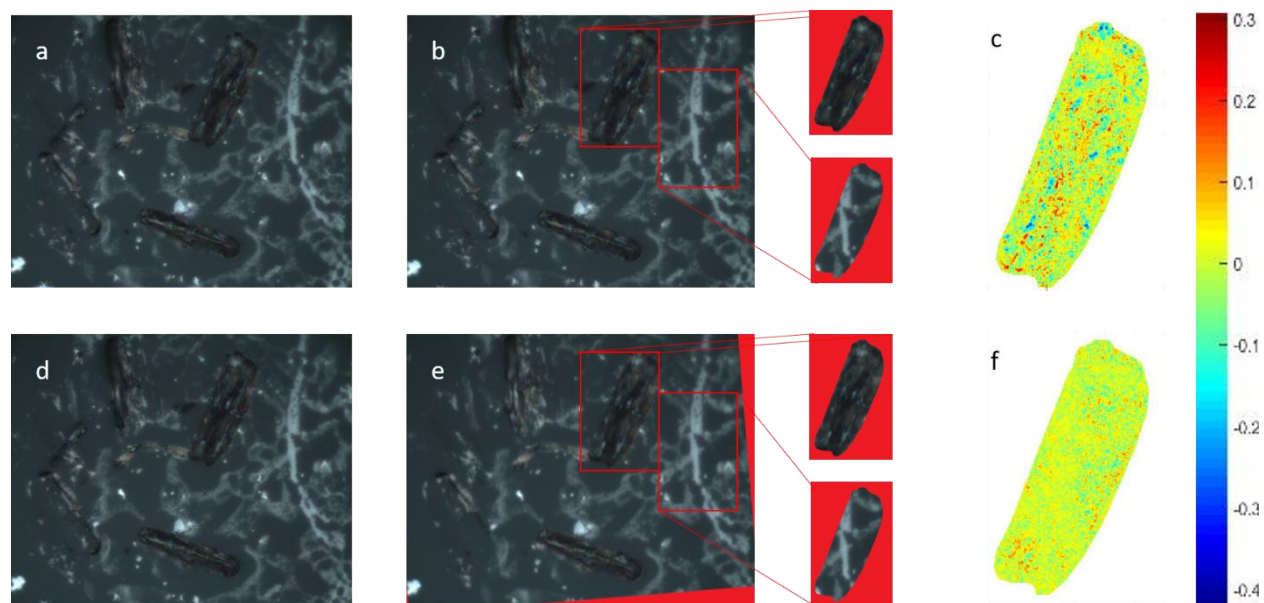
Figure 9: The progression of image analysis. The pre-assay (a) and post-assay (d) images were taken from the CCD. The post-assay image was then rotated (e) to align with the pre-assay (b) before having an area on diatom and on glass cropped out and placed on a red background. The ratio difference for diatom (c) and glass (f) are shown with a common color bar scale.

Colorimetric sensing is advantageous due to the ease with which detection can be achieved. With just a camera and a processor, detection of low levels of analytes were achieved. This facile approach is ideal for non-trained individuals and for point-of-care detection. By integrating this with a cell phone and a magnifying apparatus, an individual would be able to perform this detection thereby avoiding long delays and high costs of laboratories. Additionally, no optical labels were needed for this sensing mechanism allowing for greater ease-of-use.

3. Diatom Based Surface-Enhanced Raman Spectroscopy

3.1 Simulation of SERS Enhancement from Photonic Crystal-like Frustule

To explore the SERS enhancement due to the photonic crystal nature of frustules, the structure was simulated using Rsoft to perform a finite-difference time-domain (FDTD) analysis of the structure. The simulation was performed by Erwen Li, a member of our research group. The simulation structure was created based on the dimensions found in the SEM image of a diatom frustule found in figure 10.
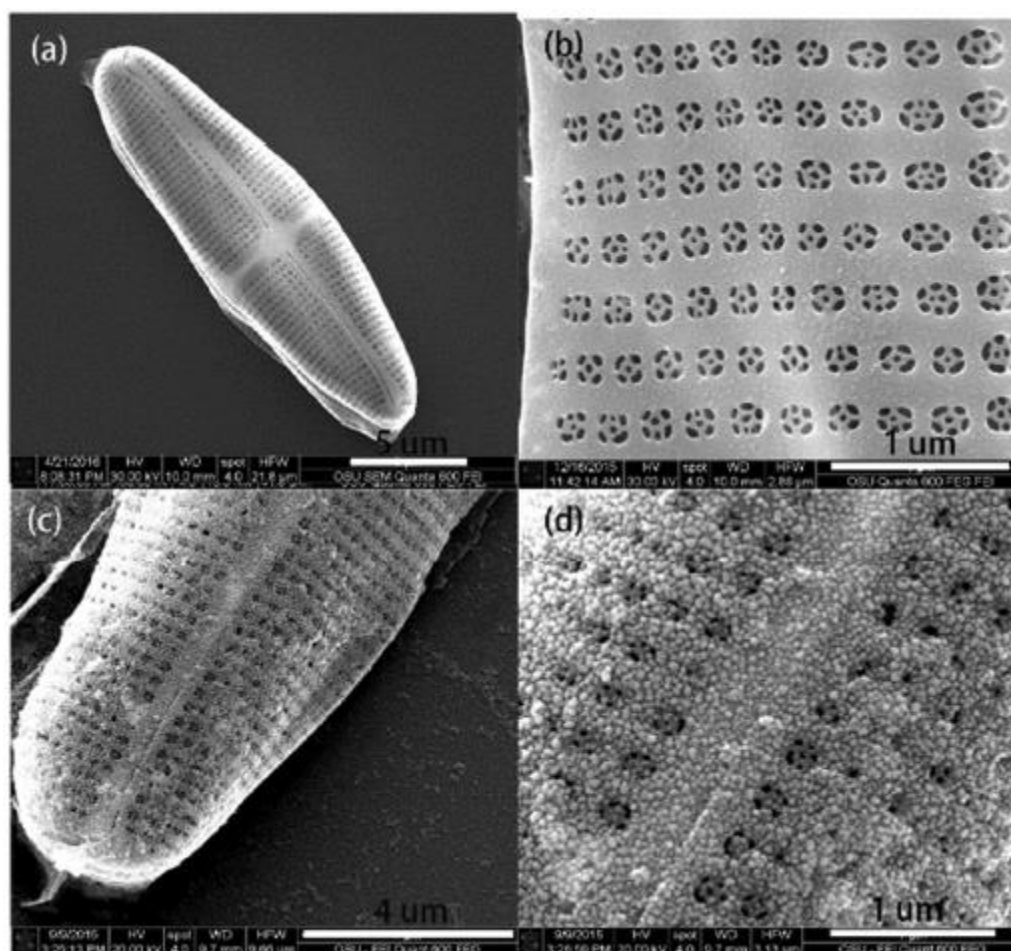
Figure 10: SEM image of (a) an overview of a single frustule, (b) arrays of pores on a frustule, (c) and (d) deposited NP seeds on the diatom frustule *via* an *in situ* growth method[52].

The structure was simulated using two layers of silicon. The top layer contains the main pore (200 nm diameter and 120 nm deep) and the bottom layer is used to simulate the five-pore structure seen at the bottom of the pore (60 nm deep). The period of the pores is 400 nm in a square pattern. Nanoparticles (NPs) 40 nm in diameter were used to enhance the Raman signal and were randomly distributed on the surface and in the pores of the diatom. This enhancement is achieved as localized surface plasmons (LSPs) form on the surface of the metal NPs due to the NPs' absorption of incident light.   The LSPs create hotspots which experience a much higher

electric field and have greater interaction with the target analyte, thus creating a stronger Raman signal. The simulated structure with the distributed NPs is shown in figure 11 (a).
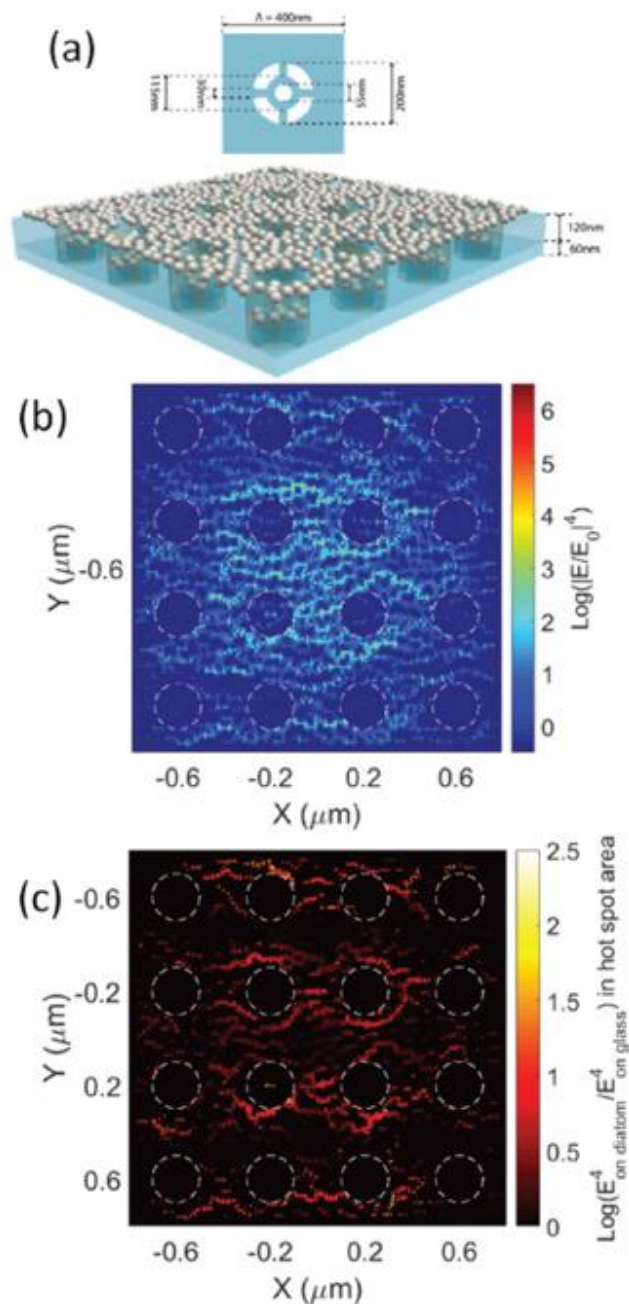
Figure 11: (a) Schematic of the 3-D simulated hybrid diatom–NP nanostructures: NPs are randomly distributed on a diatom frustule; (b) 3-D FDTD simulation of the field enhancement $|E/E0|^4$ of the nanostructure; and (c) enhancement factor of the hot-spots compared with those of NPs on a flat glass substrate. Note: the value of $|E/E0|4$ is plotted in the log-scale[52].

The structure was excited using a Gaussian beam at 532 nm with a beam diameter of 1.5 μm. This is in accordance with the beam used in our experimental results. The SERS enhancement factor is proportional to the fourth power of the electric field[53] (E^4). The electric field was normalized to the incident field and plotted in a log scale in figure 11 (b). The enhancement from the photonic crystal nature of the diatom was explored by randomly distributing the NPs on a silicon slab with the same dimensions and NP distribution as on the diatom structure. The E^4 on diatom was divided by the E^4 on silicon and plotted on a log scale in figure 11c. By placing the NPs on the diatom, the hotspots created by the interaction of the NPs experience an even greater enhancement. Most hotspots are enhanced by 10× while some are enhanced by as much as 100×. The enhancement of the hotspots leads to an enhancement in the Raman signal.

3.2 Fabrication of Diatom Based SERS Sensor

The diatom based SERS substrate was prepared by first populating a glass substrate with diatoms as described in the previous chapter. Next, the substrate was immersed in 1% Poly(diallyldimethylammonium chloride) (v/v) in Milli-Q deionized water for 45 minutes to deposit positively charged amine groups on the surface of the substrate. This allows better adhesion between the NPs and the substrate. After 45 minutes the substrate was thoroughly rinsed with deionized water. The amine functionalized substrate was then immersed in Au NP solution which had been synthesized according to the process described in the previous colorimetric chapter. The substrate was immersed in the NP solution overnight. The substrate

was again rinsed and kept in water for future use. When the substrate was to be used, pure nitrogen was used for drying.

3.3 Application to the Detection of Organics in Simulant Martian Soil

Finding life on Mars has been a topic that has received a lot of interest in the past couple years. Probes are sent to Mars to collect soil samples and run experiments in an effort to detect organic matter that would suggest past or present life on the red planet. So far, no conclusive evidence has been found to prove life on Mars but recently it has been suggested that one of the detection methods used, gas chromatography mass spectroscopy, is inaccurate due to the perchlorates in the Martian soil[54]. To prove the merit of our diatom-based SERS substrate, we detected organic matter in simulant Martian soil in the presence of magnesium perchlorate ($Mg(ClO_4)$).

Soil samples were taken from the Mojave Desert where the extreme temperatures and lack of moisture are good representations of Martian soils. Soil samples were known to have an organic concentration of 1 part-per-million (ppm). We mixed two solutions: one without $Mg(ClO_4)$ and one with. The first solution was prepared by mixing 2.3 g soil with 2.3 g of deionized water. The second was prepared by adding 23 mg of $Mg(ClO_4)$ to the first solution. Both solutions were mixed vigorously, placed in a syringe and filtered using a 1 μm syringe filter. The filtered solutions were then diluted to desired concentrations and 2μL of each solution were placed on SERS substrates and allowed to evaporate at room temperature. The SERS signal was then measured

using a Horiba Jobin Yvon Lab Ram HR800 Raman microscope with a 785 nm excitation beam averaged over two seconds and averaged over two measurements.

3.4 Organic Sensing Results

SERS measurements were first done using the soil solution without $Mg(ClO_4)$ on the diatom and on glass to validate the enhancement from diatom. The solution was diluted to get an organic concentration of 10 parts-per-billion (ppb). The solution was drop casted onto the substrate and then the SERS signal was measured on diatom and on glass. The resulting spectra are shown in figure 12. The peaks at 1374 cm^{-1} and 1574 cm^{-1} correspond to the carbon D and G-bands respectively. We see that there is a 2× peak enhancement from the diatom substrate when compared to the glass substrate, and thus highlighting the advantage of using the diatom based SERS substrate.
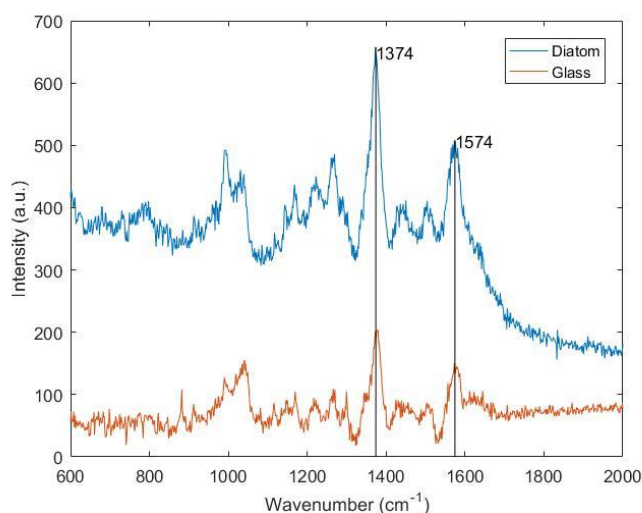
Figure 12: SERS spectra from soil solution diluted to 10 ppb on diatom and on glass[56].

We then used our diatom based sensor to detect organics in the presence of perchlorates. We followed the same procedure but used solutions with an organic concentration of 10 ppb. The spectra in figure 13 show the results. The peak at 934 cm^{-1} is a characteristic peak of magnesium perchlorate[55]. The Mg(ClO$_4$) peak is very pronounced because it is present at a concentration of 50 ppm whereas the graphite is at a concentration of 10 ppb. Even though the concentration of magnesium perchlorate is 5000× times higher, we can still detect low amounts of organic matter in the soil.
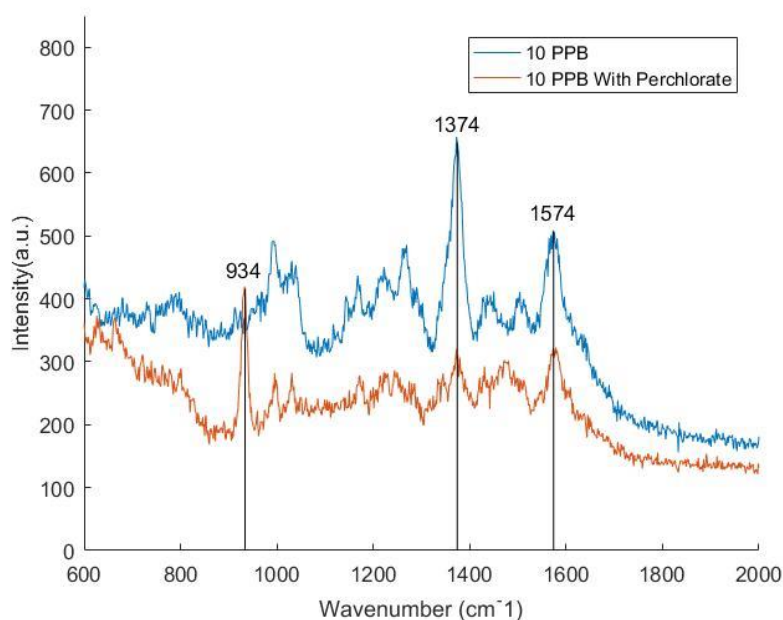
Figure 13: SERS spectra of soil with organic levels at 10 PPB in solution with and without perchlorates[56].

3.5 Discussion of SERS Enhancement from Diatom Based Sensor

We fabricated a SERS substrate based on photonic crystal-like biosilica. By using diatoms, we employed the enhanced local electric field from the photonic crystal to achieve a 2×

enhancement over the glass substrate. Furthermore, we utilized our sensor substrate to detect low levels of organic matter, down to the ppb range, in Martian simulant soil in the presence of magnesium perchlorate. The ease of fabrication and the inexpensive nature of the diatoms, along with the SERS enhancement from the diatoms, shows the practicality of our sensor.

4. Diatom Based Fluorescence Biosensing

4.1 Fluorescence Simulation of Diatom Based Biosensor

As was explained in the introduction, fluorescent biosensing performed on a photonic crystal gains signal enhancement from two physical mechanisms. The first form of enhancement is caused by guided mode resonance. Incident light upon a photonic crystal induces a resonance within the structure leading to enhanced electric fields. These resonant modes then leak out of the structure and interact with the fluorophore. This causes the fluorophore to experience a stronger excitation which, consequently, leads to stronger emission. Guided mode resonance has been theoretically and experimentally proven to occur in diatoms by our group in previous papers[49]. The second enhancement mechanism is caused by the Purcell effect. A fluorophore placed on a photonic crystal will experience an enhanced emission because of an increased density of states. To explore the enhanced emission of fluorophores on diatom surface due to the Purcell effect, we performed a finite-difference time-domain (FDTD) analysis using Lumerical's FDTD Solution package.

The structure is modelled after the Pinnularia sp. diatom which we used in our experiments. The model is comprised of a silicon dioxide slab with periodic air holes to simulate the pores. The dimensions of the simulated structure were chosen according to dimensions found from the SEM image of diatoms[33]. The pores are 160 nm in diameter with nanometer scale features at the

bottom. They are two-dimensionally periodic with a period of 300 nm along the major and minor axes of the structure. These dimensions are shown more fully on the structure in figures 14 a and c. The structure is 15 µm by 5 µm which is similar to the actual size of the diatoms and for all simulations, a mesh size of 30 nm was used.
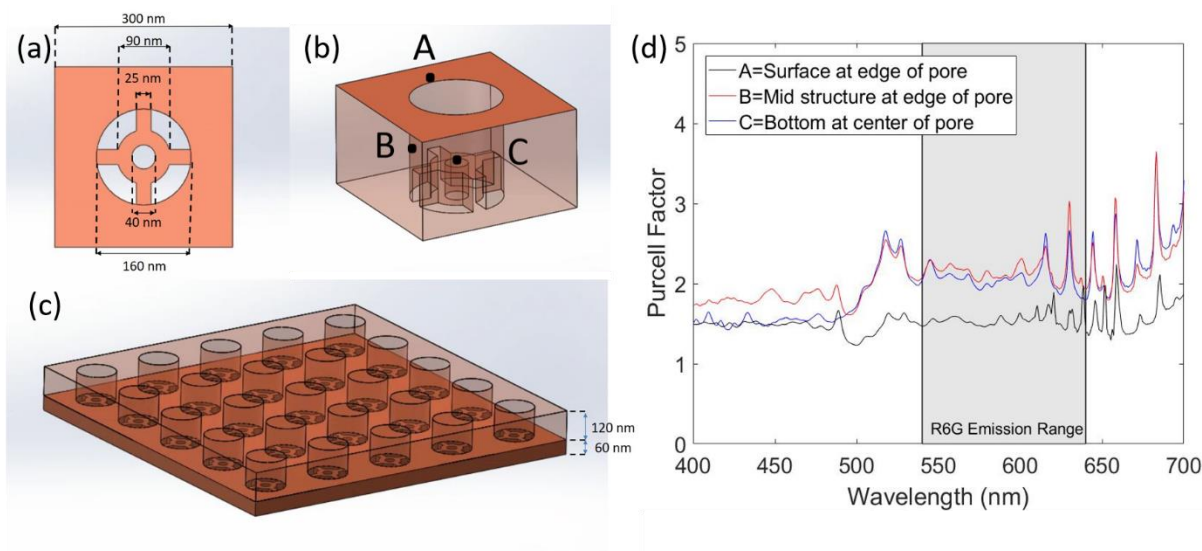
Figure 14. Simulated structure of pore (a) and (b) and 5 periods of the structure (c). The Purcell effect simulation results were simulated at three points within a unit cell with respect to wavelength (d).

To simulate the Purcell effect, a single electric dipole source was placed at various points as shown in figure 14b to excite electric fields in the structure. The Purcell Factor was calculated using Lumerical's Purcell visualization from the dipole source which is calculated as the ratio of the power emitted in the photonic crystal environment compared to that emitted in a homogenous material. In figure 14d the Purcell factor is plotted with respect to wavelength. The shaded region represents the emission region of R6G which is the fluorescent tag used in our experiment. The simulation shows that when the fluorophore is near a pore, the power emitted by a fluorophore is enhanced between 1.5 to 3× across our region of interest.

4.2 Preparation of Diatom Biosilica with Photonic Crystal Features

This section and the following preparation of diatom immunoassay substrate and immunoassay protocol sections were written by Dr. Xianming Kong in a paper that we wrote together where we were co-first authors. The schematic of the chemical process was created by him as well. Diatom (*Pinnularia sp.*) biosilica were prepared according to the method previously reported with minor modification[33]. Briefly, diatoms were cultured in a container for one week. The diatom suspension was concentrated 10× through centrifuging and dispersed in sterile filtered artificial seawater, and filtered with 20 μm mesh to separate cells. The diatom cell density was adjusted to 0.1×10^5 cells/ml for seeding. A coverslip was placed into a petri dish separately, and 15 ml of diatom cell suspension was cast onto the glass slides, and incubated in a humidifier chamber for one hour to deposit the cells on the coverslip surface. Then the coverslip with diatoms was put into a new petri dish, kept in a humidifier for 24 hours and immersed in 70% EtOH for 4 hours, and soaked in pure EtOH for 4 more hours. The diatoms were dried in air and treated in a UV ozone cleaner at 90 °C for one day. After that, the diatom substrate was ready for use.

4.3 Preparation of Diatom Immunoassay Substrate

The diatom substrate was aminated with APTES as shown in figure 15. The diatomite substrate was incubated in 15 mL of 0.05% APTES for 6 hours at room conditions followed by washing with acetone and anhydrous ethanol. After that, the aminated diatom substrate was immersed in 15

mL of 2% (v/v) glutaraldehyde (GA) in PBS for 2 hours. The GA-modified diatom was washed

thoroughly with double-distilled water three times to remove excessive GA. The GA-activated

surface was then reacted with 0.1 mg/ml of goat-anti-mouse IgG in PBS buffer at 4 ℃ for 6 hours

to get an antibody layer. After this step, 1 mg/ml of BSA was added to block the remaining GA

active surface to reduce the non-specific binding of the immunoassay. The antibody immobilized

diatom substrates were stored at 4 ℃ for future immunoassay procedures.
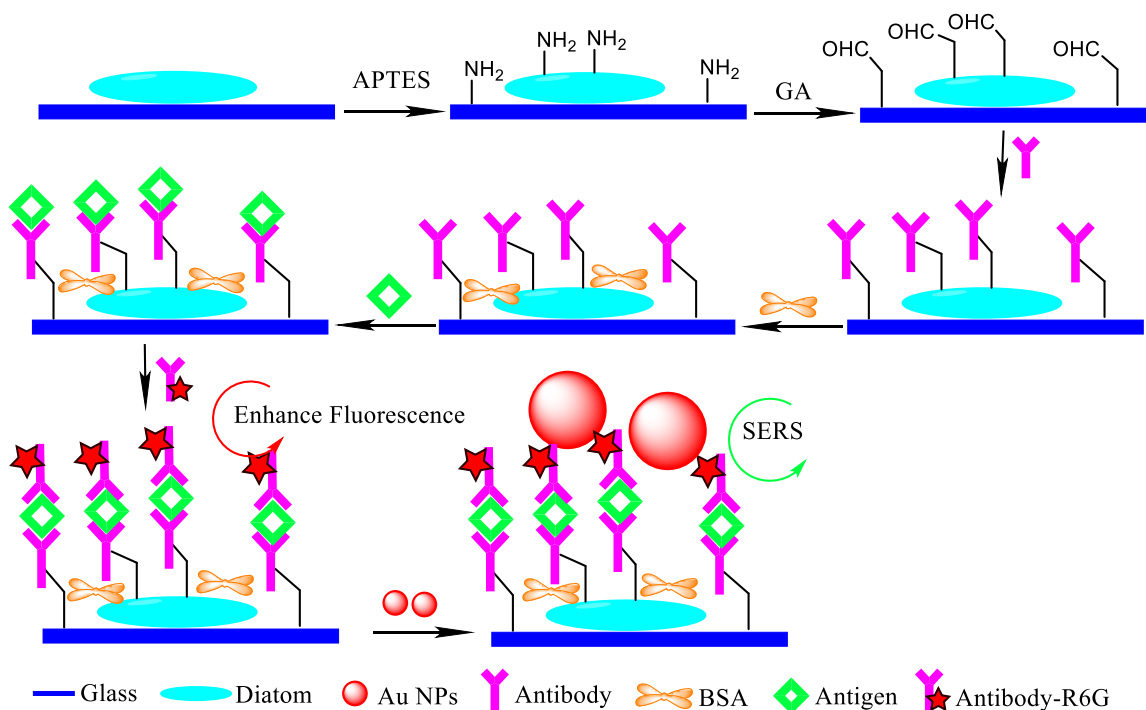
Figure 15: Schematic illustration of the dual mode immunoassay sensing on diatom photonic crystal biosilica.

4.4 Immunoassay Protocol

The immunoassay biosensing procedure is similar to a standard sandwich protocol of the

enzyme-linked immunosorbent assay (ELISA), as shown in figure 15. Briefly, 1 μL of antigen

(mouse IgG) at different concentrations was pipetted onto different spots with immobilized goat

anti-mouse IgG antibody on diatom substrate. After 2 hours immune recognition at room temperature, the substrate was rinsed with PBS buffer and water. 1 µL of goat-anti-mouse IgG labeled with R6G was pipetted onto different spots of the substrate and kept at 4 ℃ for 4 hours and washed thoroughly with PBS buffer and water, and dried by nitrogen gas for future fluorescence and SERS measurement.

4.5 Fluorescence Imaging using Diatom Based Biosensor

Fluorescence imaging operates upon the same mechanisms as fluorescent spectroscopy, in that an immunoassay procedure is performed and fluorophores are trapped upon the surface of the sensor, however the method of recording the signal differs. Rather than using an expensive spectrometer, fluorescent imaging requires only an imager, such as a camera, for signal acquisition which can be operated without the need for trained personnel. Fluorescent imaging therefore is facile and ideal for use in point-of-care applications where biosensing is required without the availability of specialized equipment or personnel. Cell phone biosensing is an application where fluorescent imaging could be used by individuals in developing countries to perform biosensing. As such, we investigated the enhancement of our diatom based biosensor to fluorescent imaging.

Fluorescent imaging was performed after the immunoassay. The immunoassay procedure was performed as described above for antigen concentrations ranging from 1 nM to 1 fM. Using a fluorescent microscope, optical and fluorescent images were taken of diatoms with varying

concentration of antigen. The fluorescent intensity fluctuates as expected with respect to the

antigen concentration as seen in figure 16.
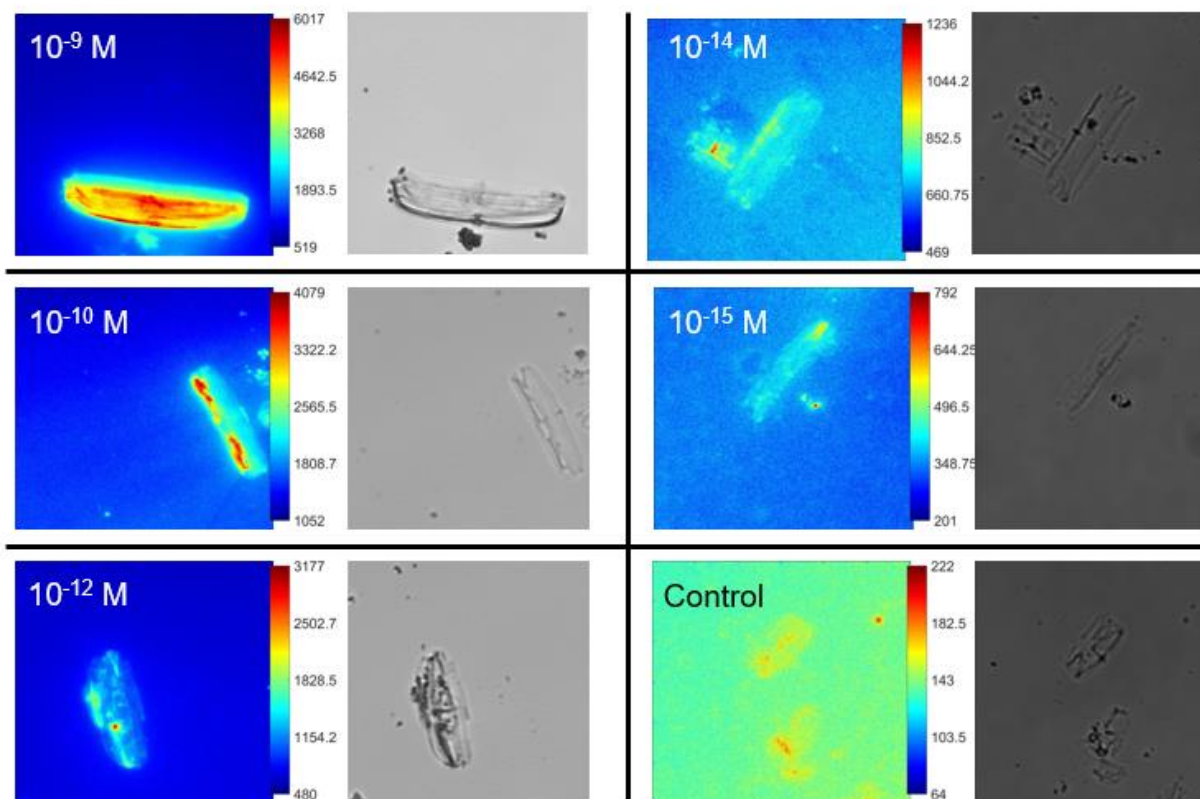
Figure 16: Fluorescent and optical images of diatoms at varying concentrations of R6G tagged mouse IgG.

The analysis of multiple images at each concentration was performed by calculating the average

pixel intensity on diatom and on glass in Matlab. The average intensities were used to compute

the enhancement due to diatom. First, the noise due to the electrical noise of our camera as well

as nonspecific binding of the antigen to our sample was determined. This was done by calculating

the average intensity on diatom of the fluorescent image for each control image. These values

were then averaged to find the average noise floor of diatoms. This process was repeated for

glass. Similar averaging was performed for each concentration and the average intensity on

diatom and on glass was found. The averages for each concentration are shown in figure 17a

and b. The enhancement factor due to diatom was calculated as the average fluorescent

intensity on diatom divided by average intensity on glass. The enhancement factor due to diatom

is shown in figure 17c. Using this methodology, we achieved detection down to 10 fM and an

intensity enhancement as high as 6×.
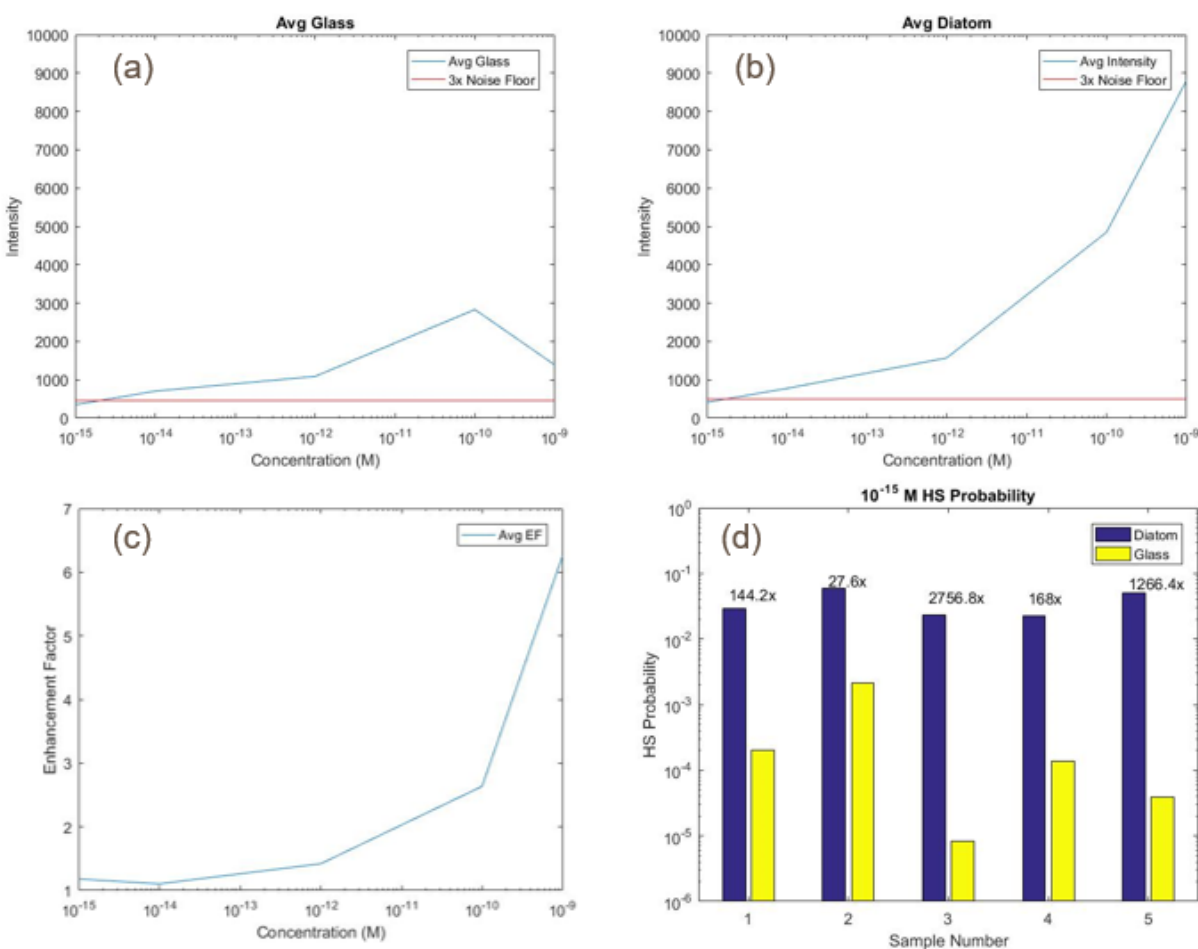
Figure 17: The average calculated intensity on glass (a) and on diatom (b). The enhancement factor calculated at each intensity(c). The hotspot probability on diatom and glass with the enhancement factor(d).

At higher concentrations, the analyte is abundant and is considered to be uniformly dispersed

across the sample. However, at the concentration of 1 fM and below, the density of fluorophores

is closer to single molecule levels. At this concentration, the molecules are no longer uniformly dispersed and by averaging the whole diatom, we dilute the strength of the fluorescence signals. As a more accurate method, a hotspot analysis was performed rather than analyzing the average intensity. A hotspot was defined as a pixel that is three times the noise floor. Counting the number of hotspots, the probability that a pixel is a hotspot is calculated on the glass and the diatom, respectively. As is shown in Figure 17d, the probability of finding a hotspot on diatom is significantly greater than that found on the glass. The enhancement due to the diatom ranges from 27× up to 2,700×. This is due to the combined enhancement from guided mode resonance and the Purcell effect.

Additionally, the emission intensity of fluorophores on and off diatoms were compared. This was done by measuring the average maximum intensity of several fluorophores on diatom and on glass. The enhancement factor was calculated by dividing the average peak intensities on diatom by the average peak intensities on glass. Following this procedure, an enhancement of 1.2× was achieved. This is comparable to the simulated Purcell effect found for fluorophores on the surface of a diatom near a pore. A combination of enhanced emission intensity as well as the increased hotspot probability leads to a limit of detection for fluorescent imaging an order of magnitude lower than sensors without the diatom based biosensor.

5. Conclusion

In conclusion, diatoms are a type of algae with a biosilica shell called a frustule. The porous nature of their biosilica frustule acts as a natural photonic crystal. Unlike most photonic crystals used in biosensors, these photonic crystals do not require any expensive or complicated fabrication processes and are abundant in nature. The photonic properties of the diatoms cause light to interact differently with the analyte helping us achieve enhanced optical signals. We have used the diatom frustules as a way to enhance multiple modalities of optical biosensors. A diatom based colorimetric sensor has been demonstrated with a limit of detection of 100 μg/mL with a signal enhancement of 5× for facile detection with a camera. We showed that our diatom based SERS sensor was able to detect organic components in simulant Martian soil in the presence of competing molecules and enhanced the signal 2×. Lastly, we have demonstrated that diatoms are capable of enhancing the fluorescent signal of a fluorophore by as much as 6× and lowering the limit of detection by an order of magnitude to 1 fM for fluorescent imaging. Our diatom-based optical biosensors have been applied to multiple-modalities of detection and have enhanced the colorimetric, SERS and fluorescent signals. The integration of diatoms into biosensors allows the sensor to be more versatile in its application and more sensitive in its detection making diatoms an excellent candidate for biosensor substrates.

6. References

1. Simionian, Good, Wang and Wild, "Nanoparticle-based optical biosensor for the direct detection of organophosphate chemical warfare agents and pesticides", Analytica Chimica Acta 534 (2005), 69-77.
2. Bohunicky and Mousa, "Biosensors: the new wave in cancer detection", Nanotechnology, Science and Applications 4 (2011), 1-10.
3. Tschmelak, Proll, and Gauglitz, "Optical biosensor for pharmaceuticals, antibiotics, hormones, endocrine disrupting chemicals and pesticides in water: Assay optimization process for estrone as example", Talanta 65 (2005), 313-323.
4. Ou, Jin, Chu, Jiang, and Yu, "Sensitive and Visual Detection of Sequence-Specific DNA-Binding Protein via a Gold Nanoparticle-Based Colorimetric Biosensor", Analytical Chemistry 82 (2010), 6015-6024.
5. Li, Guo, Ping, Liu, Zhang, Guan, Sun, and Zhang, "Visual detection of organophosphorus pesticides represented by mathamidophos using Au nanoparticles as colorimetric probe", Talanta 87 (2011), 93-99.
6. Knecht and Sethi, "Bio-inspired colorimetric detection of Hg^{2+} and Pb^{2+} heavy metal ions using Au nanoparticles", Analytical and Bioanalytical Chemistry 394 (2009), 33-46.
7. Zhang, Chen, Cheng, Zhang and Chen, "Highly Sensitive on-site detection of glucose in human urine with naked eye based on enzymatic-like reaction mediated etching of gold nanorods", Biosensors and Bioelectronics 89 (2017), 932-936.
8. Chun, Park, Han, Jang, and Yoon, "Paper-based glucose biosensing system utilizing a smartphone as a signal reader", BioChip Journal 8 (2014), 218-226.
9. Liang, Park, and Yoon, "Rapid and reagentless detection of microbial contamination within meat utilizing a smartphone-based biosensor", Scientific Reports 4 (2014).
10. Salles, Meloni, de Araujo, and Paixao, "Explosive colorimetric discrimination using a smartphone, paper device and chemometrical approach", Analytical Methods 6 (2014), 2047-2052.
11. Nie and Emory, "Probing Single Molecules and Single Nanoparticles by Surface-Enhanced Raman Scattering," Science, 275(1997), 1102-1106
12. Kneipp, Wang, Kneipp, Perelman, Itzkan, Dasari, and Feld, "Single Molecule Detection Using Surface-Enhanced Raman Scattering (SERS)", Physical Review Letters, 78(1997), 1667-1670.
13. Zheng, Li, Jurevic, Cushing, Liu and Wu, "A gold nanohole array based surface-enhanced Raman scattering biosensor for detection of silver(I) and mercury(II) in human saliva", Nanoscale 7 (2015), 11005-11012.
14. Haynes, McFarland, and Van Duyne, "Surface-Enhanced Raman Spectroscopy", Analytical Chemistry (2005), 338-346.
15. Yang, et al., "Guided-Mode Resonance Grating with Self-Assembled Silver Nanoparticles for Surface-Enhanced Raman Scattering Spectroscopy", Photonics 1 (2014), 380-389.

16. Kong, et al., "Detecting explosive molecules from nanoliter solution: A new paradigm of SERS sensing on hydrophilic photonic crystal biosilica", Biosensors and Bioelectronics 88 (2016), 63-70.

17. Shafer-Peltier, Haynes, Glucksberg, and Van Duyne, "Toward a Glucose Biosensor Based on Surface-Enhanced Raman Scattering", JACS 125(2003), 588-593.

18. Ngo, Wang, Fales, and Vo-Dinh, "Label-Free DNA Biosensor Based on SERS Molecular Sentinel on Nanowave Chip", Analytical Chemistry 85 (2013), 6378-6383.

19. Das, et al., "Fabrication of large-area ordered and reproducible nanostructures for SERS biosensor application", Analyst 137 (2012), 1785-1792.

20. Tripp, Dluhy, and Zhao, "Novel nanostructures for SERS biosensing", Nanotoday 3 (2008), 31-37.

21. Li, Wang, Guo, Wang, Ma, Ren, Du, and Wei, "A 'turn-off' fluorescent biosensor for the detection of mercury (II) based on graphite carbon nitride", Talanta 162 (2017), 46-51.

22. Du, Liu, Lou, Zhao, Wang, Xue, Zhao and Xu, "Highly Sensitive and Selective Chip-Based Fluorescent Sensor for Mercuric Ion: Development and Comparison of Turn-On and Turn-Off Systems", Analytical Chemistry 84 (2012), 8060-8066.

23. Wei, Qiang, Ren, Ren, Tang, and Meng, "Fluorescence turn-off detection of hydrogen peroxide and glucose directly using carbon nanodots as probes", Analytical Methods 6 (2014), 1922-1927.

24. Zhou, Pivarnik, Auger, Rand, and Letcher, "A compact fiber-optic immunosensor for Salmonella based on evanescent wave excitation", Sensors and Actuators B 42 (1997), 169-175.

25. Demarco, Saaski, McCrae, and Lim, "Rapid Detection of Escherichia coli O157:H7 in Ground Beef Using a Fiber-Optic Biosensor", Journal of Food Protection 62 (1999), 711-716.

26. Huang, et al., "Application of Photonic Crystal Enhanced Fluorescence to Cancer Biomarker Microarrays", Analytical Chemistry 83 (2011), 1425-1430.

27. Hsieh, Chiu, Lin, Chang, Chang and Chiang, "Amplification of the Signal Intensity of Fluorescence-Based Fiber-Optic Biosensors Using a Fabry-Perot Resonator Structure", Sensors 15 (2015), 3565-3574.

28. Zhou, Shen, Zhang, and Liu, "Fabrication of a Two-Dimensional Photonic Crystals Using Reactive Ion Etching", IEEE Communication Systems (2008).

29. Kim, Lee, Kim, Kwon, and Park, "Fabrication of photonic crystal structures on light emitting diodes by nanoimprint lightography", Nanotechnology 18 (2007), 1-5.

30. Campbell, Sharp, Harrison, Denning, and Turberfield, "Fabrication of photonic crystals for the visible spectrum by holographic lithography", Nature 404 (2000), 53-56.

31. Divliansky, Mayer, Holliday, and Crespi, "Fabrication of three-dimensional polymer photonic crystal structures using single diffraction element interference lithography", Applied Physics Letters 82 (2003), 1667-1669.

32. Deubel, Freymann, Wegener, Pereira, Busch, and Soukoulis, "Direct laser writing of three-dimensional photonic-crystal templates for telecommunications", Nature Materials 3 (2004), 444-447.

33. Deubel, Wegener, Linden, Feymann, and John, "3D-2D-3D photonic crystal heterostructures fabricated by direct laser writing", Optics Letters 31 (2006), 805-807.

34. Fenzl, Hirsch, and Wolfbeis, "Photonic Crystals for Chemical Sensing and Biosensing", Angew. Chem. Int. Ed. 53 (2014), 3318-3335.

35. Purcell, "Spontaneous Emission Probabilities at Radio Frequencies", Physical Review 69 (1946), 681.

36. Kleppner, "Inhibited Spontaneous Emission", Physical Review Letters 47 (1981), 233-236.

37. Ganesh, et al., "Enhanced fluorescence emission from quantum dots on a photonic crystal surface", Nature Nanotechnology 2 (2007), 515-520.

38. Shafiee, et al., "Nanostructured Photonic Crystal Biosensor for HIV Viral Load Measurement", Scientific Reports 4 (2014), 1-7.

39. Ye, Rong, Gu, Xie, Cheng, Zhao, and Gu, "Bioinspired angle-independent photonic crystal colorimetric sensing", Chemical Communications 49 (2013), 5331-5333.

40. Gale, Gutu, Jiao, Chang, and Rorrer, "Photoluminescence Detection of Biomolecules by Antibody-Functionalized Diatom Biosillica", Advanced Functional Materials 19 (2009), 926-933.

41. Lin, Kunduru, Bothara, Rege, Prasad and Ramakrishna, "Biogenic nanoporous silica-based sensor for enhanced electrochemical detection of cardiovascular biomarkers proteins", Biosensors and Bioelectroncs 25 (2010), 2336-2342.

42. De Stefano, Ritoroti, De Stefano, Lamberti, Lettieri, Setaro, and Maddalena, "Marine diatoms as optical biosensors", Biosensors and Bioelectronics 24 (2009), 1580-1584.

43. Delalat, Sheppard, Ghaemi, Rao, Prestidge, McPhee, Rogers, Donoghue, Pillay, Johns, Kroger, and Voelcker, "Targeted drug delivery using genetically engineered diatom biosilica", Nature Communications 6 (2015), 1-11.

44. Losic, Yu, Aw, Simovic, Thierry and Addai-Mensah, "Surface functionalisation of diatoms with dopamine modified iron-oxide nanoparticles: toward magnetically gruided drug microcarriers with biologically derived morphologies", Chem. Commun. 46 (2010), 6323-6325.

45. Aw, Simovic, Yu, Addai-Mensah and Losic, "Porous silica microshells from diatoms as biocarrier for drug delivery applications", Powder Technology 223 (2012), 52-58.

46. Parkinson and Gordon, "Beyond micromachining: the potential of diatoms", Trends in Biotechnology 17 (1999), 190-196.

47. Drum and Gordon, "Star Trek replicators and diatom nanotechnology", TRENDS in Biotechnology 21 (2003), 325-328.

48. Fuhrmann, Landwehr, Rharbi-Kucki and Sumper, "Diatoms as living photonic crystals", Applied Physics B 78 (2004), 257-260.

49. Ren, Campbell, Wang, Rorrer and Wang, "Enhancing surface plasmon resonances of metallic nanoparticles by diatom biosilica", Optics Express 21 (2013), 15308-15313.

50. Yang, Ren, Le, Campbell, Rorrer and Wang, "Surface-enhanced raman scattering immuno-assay using diatom frustules", Lasers in Electro-Optics CLEO (2014).

51. Grabar, Freeman, Hommer and Natan, "Preparation and Characterization of Au Colloid Monolayers", Analytical Chemistry 67 (1995), 735-743.

52. Kong, Xi, LeDuff, Li, Liu, Cheng, Rorrer, Tan and Wang, "Optofluidic sensing from inkjet-printed droplets: the enormous enhancement by evaporation-induced spontaneous flow on photonic crystal biosilica", Nanoscale, 8 (2016), 17285-17294.

53. Aikens, Madison and Schatz, "Raman spectroscopy: The effect of field gradient on SERS", Nat. Photonics, 7 (2013), 508-510.

54. Kate, "Organics on Mars?", Astrobiology, 10(2010), 589-603.

55. Ruan, Wang and Gu, "Surface-enhanced Raman scattering for perchlorate detection using cystamine-modified gold nanoparticles", Analytica Chemica Acta, 1 (2006), 114-120.

56. Squire, Kong, LeDuff, Rorrer, Tang, Chen, McKay, Navarro-Gonzalez and Wang, "Detection of Organic Matter in Simulant Martian Soil using Plasmonic-Biosilica SERS Substrate", Frontier in Optics 2016, OSA Technical Digest (online) (Optical Society of America, 2016).